ROTATION-INDUCED ELECTROSTATIC-POTENTIAL AND ITS EFFECTS ON THE ELECTRIC FIELD, IMPURITY DENSITY AND RADIATED POWER DENSITY ASYMMETRIES IN NSTX

L. F. DELGADO-APARICIO
Princeton Plasma Physics Laboratory (PPPL)
Princeton, NJ, USA
Email: ldelgado@pppl.gov

R. E. Bell[1], G. J. Kramer[1], M. Podestà[1], B. P. LeBlanc[1], A. Diallo[1], S. Gerhardt[1], H. Yamazaki[1,2], Y. Takase[2] and M. Ono[1]
[1]Princeton Plasma Physics Laboratory (PPPL), Princeton, NJ, 08540, USA
[2]The University of Tokyo, Graduate School of Frontier Sciences, Kashiwa 277-8561, Japan

Abstract

The computation of rotation-induced electrostatic potentials is being used to study the associated two-dimensional distribution of impurity density and radiated power density asymmetries in NSTX. This calculation relies on flux-surface quantities like T_e, T_i and ω_ϕ. The iterative process finds the 2D density profiles and the electrostatic potentials ($\Delta\varphi(R,Z)$) self-consistently assuming poloidal variation due to centrifugal forces. The depth of the potential well can reach -110 to -280 V for core NSTX rotation between 180-360 km/s but remains very small if one compares with the core plasma potential (e.g. few kilo Volts) or the energy of fast ions (e.g. few to several tens of keV). The net-change of the plasma potential and radial electric field is of the order of just 5-6% and in accordance with a simple theoretical calculation. This computation is being used to increase our understanding of asymmetries and the reduction of Z-peaking, to examine the effect of $\Delta\varphi$ possibly modifying the heat and particle transport through changes in the **E**×**B** shear, radiation asymmetries before tearing mode onsets, as well as to aid the design of new diagnostics for NSTX-U.

1. INTRODUCTION AND MOTIVATON

With the selection of molybdenum and tungsten for the divertor in fusion experiments, the importance of understanding the sources, transport and confinement of high-Z impurities has become crucial. In particular, modify and attempt to control high Z-transport to avoid core accumulation is necessary to achieve and maintain high fusion performance in long-pulse scenarios. Understanding the role of poloidal asymmetries for reducing the impurity peaking is highly desirable for the development of the spherical tokamak (ST) concept. An important impurity transport task for NSTX-U will be thus to characterize the properties of H-mode scenarios with high toroidal velocities, in which the 'standard' neoclassical theory [1] derived for 'subsonic' Mach numbers may no longer be applicable [2-4].

The main motivation behind the installation of the new higher-tangency-radius neutral-beam injectors in NSTX-U [see Fig 1-a)] was to increase the available heating power, the NBI-driven current and the bootstrap fraction. However, the use of tangential off-axis beams may bring a concomitant increase of the deuterium and impurity Mach numbers providing additional momentum to the outward low temperature plasma [see Fig 1-b)]. In this scenario, the formation of a rotation-induced electrostatic potential ($\Delta\varphi(R,Z)$) with changes in the radial electric field (E_r) and the appearance poloidal density asymmetries [2-4] are nearly assured. The computation of these electrostatic potentials is currently being used to study the associated two-dimensional distribution of impurity density and radiated power asymmetries in NSTX and NSTX-U. The Mach number correction enhancing the impurity asymmetries is proportional to the ion-mass so the effects on high-Z impurities

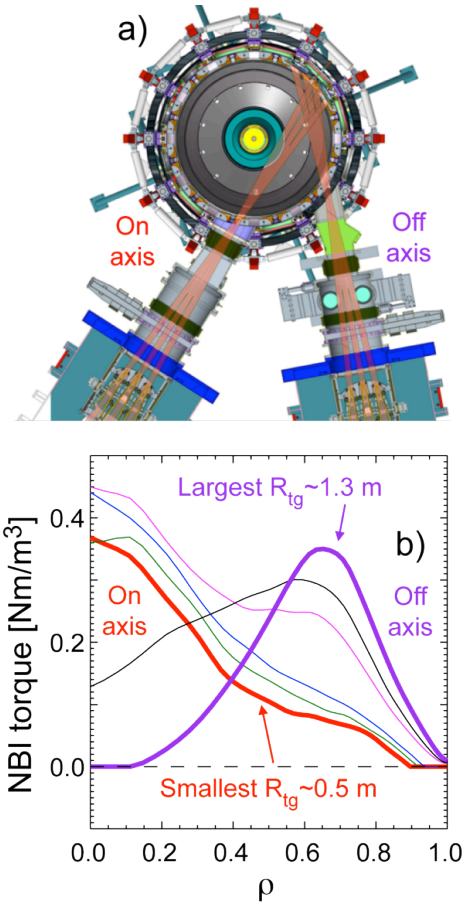

Fig. 1. NSTX-U's tangential NBI system and expected torque.

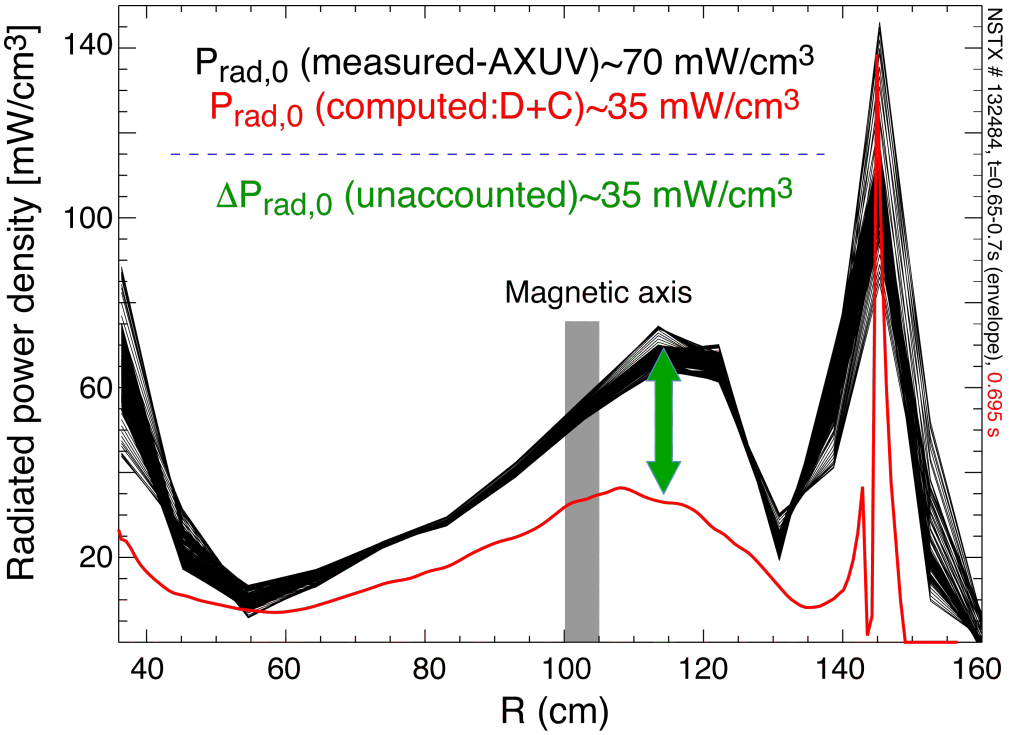

Fig. 2. P_{rad} shortfall and in/out asymmetry in NSTX.

such as Fe_{26}, Mo_{42} and/or W_{74} will be easily distinguishable from that of Li_3, Be_4, B_5 or C_6. It has also been theorized that formation of these potential differences and subtle changes in background radial electric field (E_r) can possibly vary the heat and particle transport by increasing the fraction of trapped particles [3] and modifying the linear/non-linear stability of gradient-driven modes due to changes in the **E**×**B** shearing rates [5], but these findings remain to be evaluated experimentally.

2. PHYSICS MEASUREMENTS AND MAPPING IN FLUX SURFACES

The main centrifugal effect of toroidal rotation on heavy impurities is their radial displacement to the outer plasma, which result in a non-uniform distribution around a magnetic flux-surface. This effect has already been observed in NSTX as is shown in Figure 2. The radiated power at the low-field-side (LFS, R=120 cm) is higher than at its correspondent radii at the high field side (HFS, R~80 cm) possibly due to an asymmetric poloidal distribution of medium–Z impurities (e.g. Fe, Ni) sputtered from the vacuum vessel or RF antennae limiters.

The main motivation for performing this study is to find a reliable model to characterize the transport properties of low-density H-mode scenarios with high toroidal velocities in which the '*standard*' neoclassical theory (e.g. NCLASS) derived for 'subsonic' Mach numbers may no longer be applicable. The transport equations retaining strong

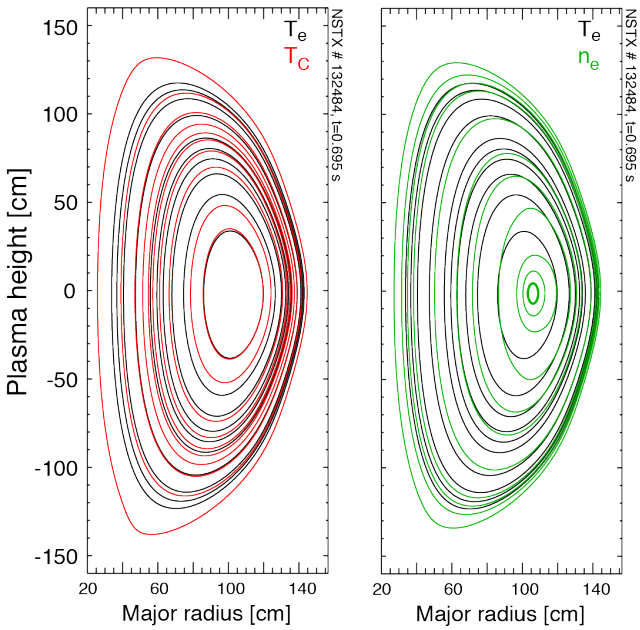

Fig. 3. a) Nested electron and ion temperatures and b) electron density offset from ψ(R,Z).

rotation ($V_\phi \sim V_{th}$) with intrinsic high Mach-numbers were first derived by Hinton and Wong via extension of Hazeltine's original NCLASS treatment (see [2-4] and references therein). The density at a given flux surface can be written as [3],

$$\frac{n_j(\theta)}{n_j(\theta=0)} = \exp\left(\frac{\omega_0^2[R^2(\theta)-R^2(\theta=0)]}{2V_{th,j}^2} - \frac{eZ_j\Delta\varphi(\theta)}{T_j}\right) \quad (1)$$

where $n_j(\theta=0)$ is the impurity density profile at the equatorial-midplane at the low-field-side (LFS).

Due to the different effect of centrifugal forces on electrons, main ions and impurities, a differential electrostatic potential is generated to satisfy quasi-neutrality [3]. The calculations presented in this paper start with the mid-plane data measured by the Multi-point Thomson Scattering (MPTS) and Charge Exchange Recombination Spectroscopy (CHERS) diagnostics but relies on the appropriate mapping of flux-surface quantities like electron and ion temperature ($T_{e,C}$) and rotation frequency (ω_ϕ) to find the 2D electron, deuterium and carbon density profiles self-consistently assuming the presence of a poloidal variation due to centrifugal forces [6,7]. The few assumptions considered include a zero electron mass, a D-D plasma, fully-stripped carbon ions, a trace impurity with charge "Z" given by coronal equilibrium (<Z>(T_e)) and equilibrated ion temperatures (e.g. T_D=T_C=T_Z). As result of this numerical procedure nested electron and ion temperatures are mapped on flux surfaces $\psi(R,Z)$ while the electron density (n_e) shows a small departure from poloidal symmetry due to centrifugal effects (see Figure 3).

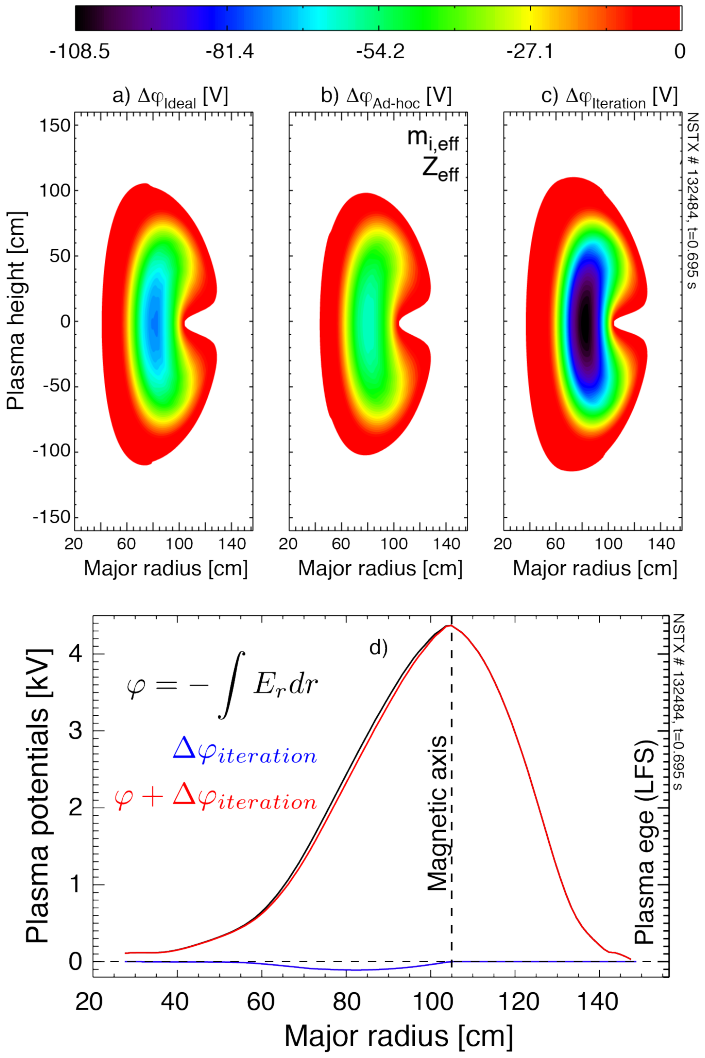

Fig. 4. a) Ideal, b) *ad-hoc* and c) iterative solutions of Δφ and its effect changing the mid-plane plasma potential.

3. ELECTROSTATIC POTENTIAL AND CHANGES OF THE RADIAL ELECTRIC FIELD (Er)

The ideal, *ah-hoc* and numerical iterative solutions for the electrostatic potential difference [$\Delta\varphi=\varphi(\theta)-\varphi(\theta=0)$] and changes on the radial electric field are now routinely obtained as depicted in Fig 4. The ideal electrostatic potential shown in Fig. 4-a) is used only as a reference since it is obtained assuming that the main intrinsic impurity (e.g. carbon) is at the trace limit ($\alpha_C=36n_C/n_e \ll 1$),

$$\Delta\varphi|_{\alpha_C<<1} = \frac{T_e}{T_e+T_i}\frac{m_i\omega_\phi^2}{2e}\left(R^2-R_0^{*2}\right) \quad (1)$$

where, $\omega\phi$ is the toroidal rotation frequency profile and R_0* are the references positions at the LFS mid-plane. In this limit, the minimum of the $\Delta\varphi(\theta=\pi)$ is approximately -70 V. The *ad-hoc* solution [8] shown in eq. (2) attempts

to extend the previous ideal approximation beyond the carbon trace limit [2] by assuming a finite effective plasma mass (m_{eff}) and an effective charge (Z_{eff}) but does not adequately captures the physics since the Z_{eff} dependence in the denominator reduces the depth of the potential well to -55 V,

$$\Delta\varphi|_{eff} = \frac{T_e}{Z_{eff}\cdot T_e + T_i}\frac{m_{eff}\omega_\phi^2}{2e}\left(R^2 - R_0^{*2}\right) \quad (2)$$

The iterative solution for the electrostatic potential from the measured carbon density and central toroidal rotation using NSTX data is shown in Fig. 4-c) and can be calculated using arbitrary values of the core low-Z impurity strength factor which often exceeds unity ($\alpha_{C,0}>1$). The well's depth of the iteration solution is nearly 50% stronger than the ideal case and nearly twice as the *ad-hoc* approximation. A time-dependent solution (not shown here [6,7]) shows also an in/out asymmetry evolution with strong ω^2 scaling as indicated in eqns. (1) and (2). The depth of the potential well in the HFS can reach -110 to -280 V for core NSTX rotation velocities between 180 – 360 km/s but remains small if one compares with the core plasma potential (e.g. few kilovolts) or the energy of circulating and/or trapped fast ions (e.g. few tens of kilovolts).

The net-change of the plasma potential profile due to the presence of the rotation-induced electrostatic well is very small and of the order of 5-6% as is shown in Fig. 4-d). This small effect can be understood also analytically calculating the scaling of the changes of the radial electric field. The rotation-induced electrostatic potential and related change of the local electric field can be written as in eqns. (3) and (4) with *C* being a constant that normalizes the numerical iteration solutions to the ideal approximation and $L\omega_\phi$ is the gradient scale length of the toroidal rotation frequency,

$$\Delta\varphi(r,\theta=\pi) \equiv \frac{\mathcal{C}T_e}{T_e+T_i}\frac{m_i\omega_\phi^2}{2e}\left(R^2 - R_0^{*2}\right) \approx -2\mathcal{C}R_0 r\frac{T_e}{T_e+T_i}\frac{m_i}{e}\omega_\phi^2 \quad (3)$$

$$\Rightarrow \Delta E_r(r,\theta=\pi) \equiv -\nabla_r(\Delta\varphi(r,\theta=\pi)) = 2\mathcal{C}R_0\frac{T_e}{T_e+T_i}\frac{m_i}{e}\omega_\phi^2\left(1+2r/L_{\omega_\phi}\right) \quad (4)$$

The core electric field in NSTX is mainly determined by the $V_\phi B_\theta$ term [9] which can be further simplified writing $B_\theta(r) \approx rB_\phi/q(r)R$ and the toroidal field dependence as $B_\phi \sim B_{\phi,0}R_0/R$, where $B_{\phi,0}$ is the toroidal magnetic field at the magnetic axis,

$$E_r \approx V_\phi B_\theta \sim \frac{R_0 r^2}{q(r)R^2}\omega_\phi B_{\phi,0} \quad (5)$$

Using Eqns. (4) and (5), the fractional change of radial electric field for $T_e/(T_e+T_i)\sim 0.45$ is,

$$\Rightarrow \frac{\Delta E_r}{E_r}(r,\omega_\phi,\theta=\pi) \sim 0.9\mathcal{C}q(r)\left(\frac{R}{r}\right)^2\frac{w_\phi(r)}{\Omega_{i,0}}\left(1+2r/L_{\omega_\phi}\right) \quad (6)$$

where, $\Omega_{i,0}$ is the core ion gyro-frequency. The ratio of the analytic expressions for the asymmetric radial electric field to the background radial field for C=1.55, q(r)=1.4, R~80 cm, r~22.5 cm, $\omega\phi=2.15\text{x}10^4$ Hz and $\Omega_{i,0}=2.15\text{x}10^7$ Hz, is of the order of 5% which is nearly the same as the one calculated experimentally and shown in Fig. 4-d).

4. IMPURITY DENSITY (n_Z) ASYMMETRY FACTORS

The computation of rotation-induced electrostatic potentials is also being used to study the associated two-dimensional distribution of impurity density and radiated power asymmetries in NSTX and NSTX-U. This

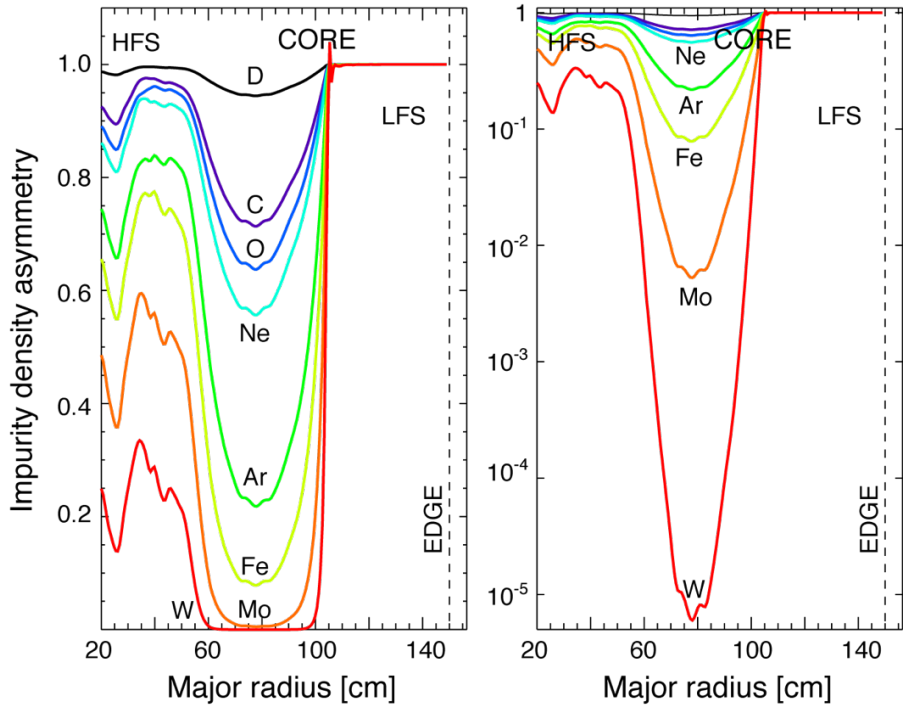

Fig. 6. Mass-dependence of asymmetry

calculation also finds 2D asymmetry factors using Eqn. (1) for impurity profiles which are at the trace limit with very small changes to quasi-neutrality and Z_{eff} (see Fig 6, in linear and logarithmic scales). While the density asymmetry remains weak (but experimentally noticeable) for low-Z impurities like Carbon, Oxygen and Neon, the asymmetry factor is very strong for higher-Z impurities like Ar, Fe, Mo and W. For the NSTX case considered here, the Molybdenum and Tungsten density holes at the high-field-side (HFS, R=80 cm) could be of the order of 1% and less than 0.01% of the density in the corresponding low-field-side (LFS).

5. RADIATED POWER DENSITY (P_{RAD}) PROFILES

The local radiated power density profiles will been modeled using hydrogenic Bremsstrahlung for the Deuterium contribution and Bremsstrahlung, radiative recombination and line-emission for the intrinsic impurities of choice (e.g. C, O, Ne, Ar, Fe, Mo and W). Any other intrinsic or extrinsic impurity (e.g. used for diagnostic purposes or impurity transport studies), with an arbitrary concentration profile, can be added to the mix. For simplicity, the estimates of average charge state and radiated power density (P_{rad}) can be made using coronal equilibrium and the cooling rate formalism. For the Deuterium case we have use $P_{rad,D} \sim n_e n_D L_D$, where $L_D = 5.35 \times 10^{-37}\ T_e^{1/2}$ [keV] Wm^3 is the hydrogenic Bremsstrahlung. For the impurities considered we have used $P_{rad,Z} \sim n_e n_Z L_Z$, where L_Z are the temperature-dependent steady state radiative cooling rates tabulated by Post [10] and Putterich [11].

The Deutrium and Carbon radiated power density 2D profiles are shown in Figs. 6-a) and b); a "cut" along the equatorial mid-plane was also used in Fig. 2 with a core peak value of 35 mW/cm^3 to showcase the P_{rad} shortfall and in/out asymmetry in NSTX. In Figs. 6-c and d) and 7, we show the core impurity radiation 2D profiles assuming the presence of Oxygen, Neon, Argon, Iron, Molybdenum and Tugnsten. Arbitrary peak density profiles have been considered for these simulations with an volume integrated radiated power for each impurity of about 0.2 MW; in comparison, the total radiated power from Deuterium and Carbon is of the order of 0.65 MW. While the asymmetry in the core radiated power from low-Z ions (e.g. O, Ne) is relatively small, the core density and radiation from medium- to high-Z's will be strongly affected by centrifugal forces (see 2D P_{rad} profiles in Fig 7). At even higher toroidal rotation, the asymmetry is stronger concentrating the Mo and W radiated power strictly to the low-field-side. Different cases of realistic impurity densities with distinct peaking factors (e.g. peaked vs flat vs hollow) profiles will be presented elsewhere [7].

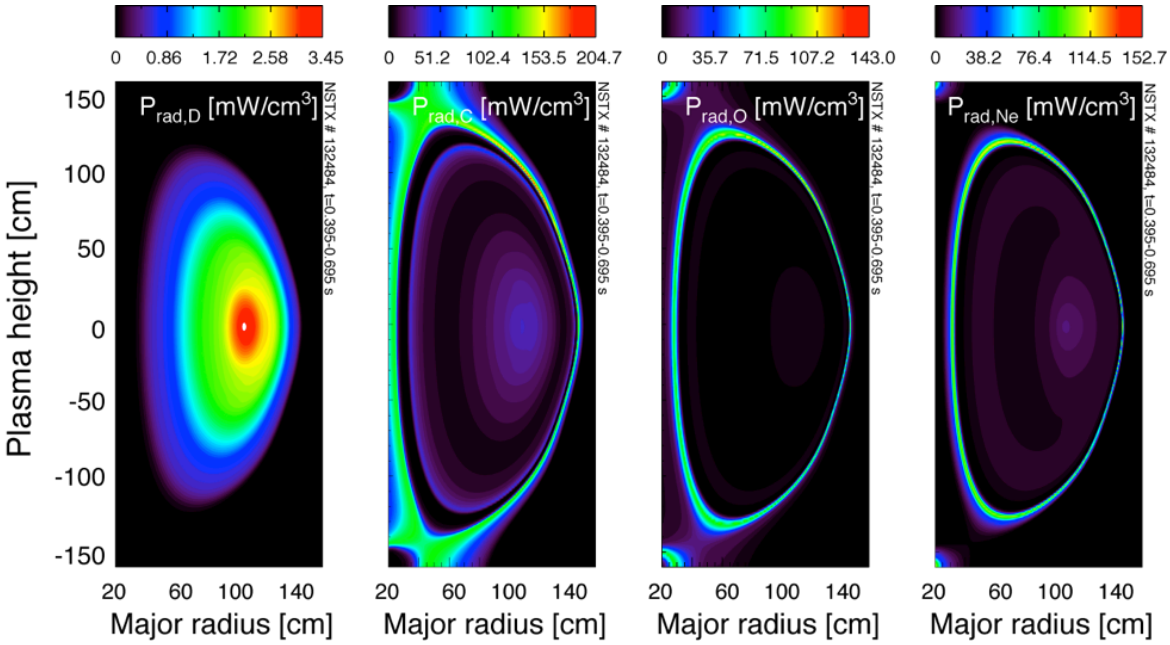

Fig. 6. Core impurity radiation from low-Z ions (e.g. Deuterium, Carbon, Oxygen and Neon) will be weakly affected by centrifugal forces.

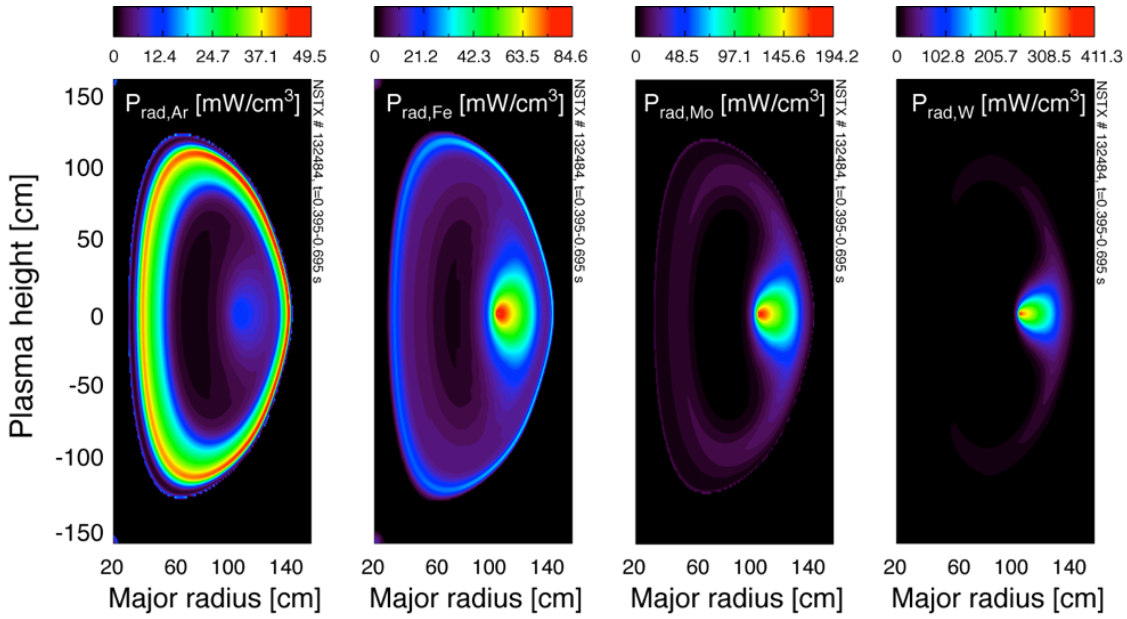

Fig. 7. Core impurity radiation from medium- to high-Z's (e.g. Argon, Iron, Molybdenum and Tungsten) will be strongly affected by centrifugal forces.

6. SUMMARY

In summary, the computation of rotation-induced electrostatic potentials is being used to study the associated two-dimensional distribution of impurity density asymmetries in NSTX. This calculation relies on flux-surface quantities like Te, Ti and $\omega\phi$. The iterative process finds the 2D density profiles and the electrostatic potentials ($\Delta\varphi$) self-consistently assuming poloidal variation due to centrifugal forces. The depth of the potential well can reach -110 to -280 V for core NSTX rotation between 180 – 360 km/s but remains very small if one compares

with the core plasma potential or the energy of fast ions. The net-change of the plasma potential and radial electric field is of the order of just 5-6% and in accordance with a simple theoretical calculation. This computation is being used to increase our understanding of asymmetries and the reduction of Z-peaking, to examine the effect of electrostatic potentials possibly changing the heat and particle transport, radiation asymmetries before tearing mode onsets, as well as to aid the design of new diagnostics for NSTX-U (e.g. ME-SXR [12], XICS, Bolometers, etc).

ACKNOWLEDGEMENTS

This work is supported by the U.S. Department of Energy, Office of Fusion Energy Sciences under contract number DE-AC02-09CH11466.

REFERENCES

[1] W. Houlberg, et al., PoP, **4**, 3320, (1997).
[2] J. A. Wesson, NF, 37, 577, (1997).
[3] E. Belly and J. Candy, PPCF, **51**, 075018, (2009).
[4] L. Delgado-Aparicio, et al., NF, **51**, 083047, (2011).
[5] A. Mollen, et al., PoP, **19**, 052307, (2012).
[6] L. F. Delgado-Aparicio, Proceedings of the 45th EPS Conference on Plasma Physics, Prague, Czech Republic, (2018)
[7] L. Delgado-Aparicio, to be submitted to NF, (2018).
[8] T. Odstrcil, et al., PPCF, **60**, 014003, (2018).
[9] R. Bell, PoP, **17**, 082507, (2010).
[10] D. E. Post and R. V. Jensen, At. Data Nucl. Data Tables, **20**, 397, (1977).
[11] T. Putterich et al., Nucl. Fusion, **50**, 025012, (2010).
[12] L. F. Delgado-Aparicio, RSI, **87**, 11E204, (2016).